IEEE Access
Multidisciplinary | Rapid Review | Open Access Journal

Received 1 November 2024, accepted 23 November 2024, date of publication 27 November 2024,
date of current version 9 December 2024.

Digital Object Identifier 10.1109/ACCESS.2024.3508575

RESEARCH ARTICLE

An Integrated Fault Detection, Classification, and Region Identification Methodology Applied to Onshore Wind Farm Collector Systems

MOISÉS J. B. B. DAVI[1], MÁRIO OLESKOVICZ[1], (Member, IEEE), AND FELIPE V. LOPES[2], (Senior Member, IEEE)
[1]Department of Electrical and Computer Engineering, University of São Paulo, São Carlos 13566-590, Brazil
[2]Department of Electrical Engineering, Federal University of Paraíba, João Pessoa 58051-900, Brazil

Corresponding author: Moisés J. B. B. Davi (moisesdavi@usp.br)

This work was supported in part by the Brazilian Federal Agency for Support and Evaluation of Graduate Education (CAPES); in part by São Paulo Research Foundation (FAPESP) under Grant 2022/00483-0; in part by the National Council for Scientific and Technological Development (CNPq) under Grant 309184/2023-1 and Grant 311547/2021-4; in part by the Research Centre for Greenhouse Gas Innovation (RCGI) hosted by the University of São Paulo (USP) sponsored by FAPESP under Grant 2020/15230-5; and in part by TotalEnergies and the strategic importance of the support given by ANP (Brazil's National Oil, Natural Gas, and Biofuels Agency) through the Research, Development, and Innovation (R&DI) Levy Regulation.

ABSTRACT This paper is motivated by the growing penetration of renewable power plants in electrical systems worldwide and the scarcity of studies evaluating fault detection, classification, and localization tasks when applied within wind farms, i.e., their collector systems. In this context, the performance of existing fault detection and classification methods is assessed using single or multiple measurement points based on a measurement management approach presented in this work. For the studies, a system with a realistic topology of onshore wind farm collectors is modeled in the PSCAD software, and several fault scenarios varying fault type, resistance, inception angle, and location are represented, besides variations in the wind farm's generation level. As the main contributions and novelties to the state-of-the-art, this paper provides: 1) pioneering insights about atypical faulty phase current behaviors in wind farm collector systems, 2) recommendations about conventional fault detection and classification methods that are most suitable for application in onshore wind farm collectors, and 3) an integrated methodology for fault detection, fault classification, and fault region identification in onshore wind farm collector systems.

INDEX TERMS Fault classification, fault detection, fault section identification, inverter-based resources, renewable generation, wind farm collectors.

I. INTRODUCTION

Over the past few years, many countries have significantly changed their electricity grids due to the growing focus on renewable energy generators [1]. A key factor driving the widespread adoption of renewable energy worldwide has been the deployment of electronic converters to overcome the inherent variability of wind and solar power. Within this context, Inverter-Based Resources (IBRs) stand out, such as type IV wind generation, also known as Full-Converter Generators (FCG) [2].

Although IBRs demonstrate operational efficiency, they pose complex challenges for protection and fault diagnosis schemes due to the unique characteristics of their fault contributions, influenced by the inverter control strategies [2], [3]. Consequently, in recent years, numerous researchers have focused on analyzing IBR fault contributions, particularly addressing impacts on traditional protection and fault diagnosis functionalities [2], [3].

Considering that most large renewable power plants are connected to transmission and sub-transmission systems,

The associate editor coordinating the review of this manuscript and approving it for publication was R. K. Saket.

several studies on IBR impacts in directional [4], distance [3] and phase selection [5] protections have been conducted, besides studies about general aspects of IBR challenges to protection systems [6].

Concerning disturbance detection methods, the precursors directly assess the currents measured in the power system and consider that a disturbance is associated with the current variations in faulted phases [7], [8]. In summary, these methods detect disturbances through changes in magnitude between the present samples and those obtained with the last sample or cycle, exceeding adjusted thresholds. There are also strategies based on specific signal processing techniques, such as the Discrete Wavelet Transform [9] and Stockwell Transform [10]. Despite allowing fast disturbance detection, the operation of these methods can be jeopardized by incorrect adjustment of sensitivity thresholds, and some proposals require higher sample rates, depending on the pre-processing strategy used.

Modern disturbance detection methods based on artificial intelligence also stand out, being often based on artificial neural networks [11], fuzzy logic [12], and other approaches. Although intelligent techniques have been employed in proposing satisfactory methodologies, it is recognized that the training/validation stages can make their practical implementation complex if not handled properly.

Regarding fault classification methods, there are the precursors based on comparing the superimposed current and fundamental zero sequence phasors [7] and those based on specific signal processing techniques [10]. Nevertheless, the operation of these methods is based on conventional synchronous generation fault contribution characteristics, i.e., significant variations are only expected in the currents and voltages of faulted phases. Furthermore, some approaches in the literature use intelligent techniques [13], [14], [15] which, although promising, require databases for the training/validation stages, as previously mentioned.

In addition, it is worth noting that all the methodologies referred to in the previous paragraphs have in common that only electrical systems with conventional generators are considered. In other words, the literature on evaluations regarding the impact of IBRs on these methods' performance is scarce. The few studies that have considered the impact of IBRs on fault classification [16], [17] and location [18] tasks, for example, have in common the focus on the method's performance for faults in the transmission line that interconnects IBRs to the grid. Therefore, studies evaluating the performance of fault detection and classification functions, focusing on fault occurrences within IBR power plants, i.e., in their collector systems, are still necessary.

In this context, recognizing the importance of this topic, the main contributions of this paper are:

- The performance of four state-of-the-art fault detection methods and six fault classification methods is evaluated when applied to diagnose faults in onshore wind farm collector systems. Recommendations about the best-performing methods are unprecedented contributions of this paper;
- The studies made it possible to identify atypical behaviors in faulted phase currents that challenge the performance of traditional fault diagnosis methods and depend on factors such as the employed measurement point and the wind farm's generation level at the fault inception instant;
- The evaluations consider the methods' decision for two different measurement approaches: 1) single measurement point on the primary of the collector transformers and 2) multiple measurements on the main collector busbars. Regarding the second approach, the integrated methodology for managing multiple measurements, enabling fault detection, classification, and region identification is the main contribution of this paper.

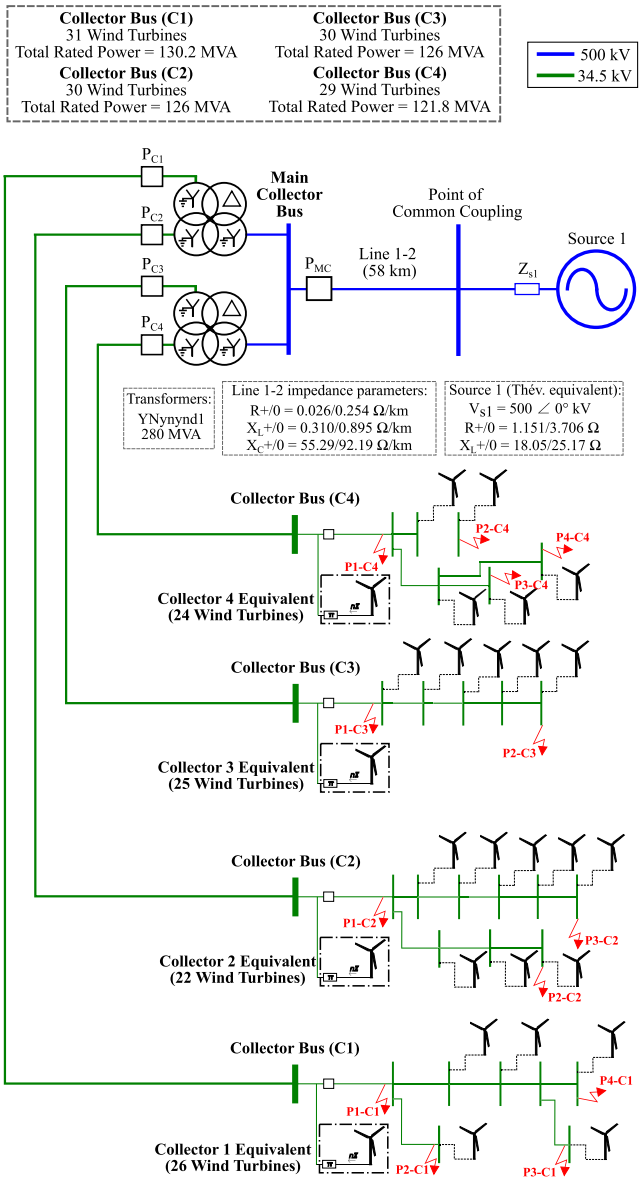

FIGURE 1. Test system single-line diagram and parameters.

The PSCAD software was employed to model a realistic wind farm and to simulate fault scenarios at different points in the collector systems. Variations in the wind farm's generation level were considered. As a result, the paper provides valuable insights and recommendations about fault diagnosis in onshore wind farm collector systems and presents a complete methodology for this purpose.

II. TEST SYSTEM

The single-line diagram and parameters of the test system are illustrated in Fig. 1. The wind farm comprises 120 FCG wind turbines, divided into four collector busbars connected to the main collector bus by two four-winding transformers with rated powers of 280 MVA. Each collector busbar consists of several wind turbine connection circuits. For this research, one circuit of each collector bus is chosen to be detailed so that faults can be applied at different points of these circuits, as indicated in Fig. 1. The remaining non-detailed circuits are represented by an equivalent circuit, following the guidelines presented in [19]. For modeling the FCG, all controls are adjusted as described in [20] and [21].

Seeking to obtain a representative database of simulated fault scenarios in the modeled wind power plant, a diversity of fault parameters were defined for the simulations, following typical variations in the technical literature regarding fault types, resistances, locations, and inception angles, as well as wind farm generation levels, to represent the inherent generation variability of these systems. Thus, short-circuits were simulated at the 13 points outlined in Fig. 1, considering variations in fault types (AG, BG, CG, AB, BC, CA, ABG, BCG, CAG, and ABC), resistances (0, 5, 10, 15, 25, 40, and 50 Ω), and inception angles (0, 45, and 90 degrees). Moreover, the wind farm's generation level in p.u. varied between 0.1, 0.25, 0.5, and 0.75. The simulations considered wind turbine operation with a unity power factor.

Therefore, considering the variations in generation level and fault parameters, 10920 scenarios are evaluated. The studies consider the measurements obtained at the main collector busbar (P_{MC}) and the collector busbars (P_{C1}, P_{C2}, P_{C3}, and P_{C4}).

III. EVALUATED FAULT DETECTORS

Four state-of-the-art fault detectors were assessed, referred to in this paper as 1) Cycle-By-Cycle (CBC) comparison method [8], 2) Sample-By-Sample (SBS) comparison method [8], 3) Cumulative Sum (CUSUM) approach [22], and 4) Current-Slope Based (CSB) detector [23].

A. CBC

This method detects faults through the difference between the present signal sample and that obtained in the previous cycle. A disturbance is detected when this difference exceeds a threshold (TH) for more than two consecutive samples [8].

TABLE 1. Decision-making rules of SCM-C.

Conditions	Fault Type
$(Is_b < k{\cdot}Is_a)$ *and* $(Is_c < k{\cdot}Is_a)$	AG
$(Is_a < k{\cdot}Is_b)$ *and* $(Is_c < k{\cdot}Is_b)$	BG
$(Is_a < k{\cdot}Is_c)$ *and* $(Is_b < k{\cdot}Is_c)$	CG
$(Is_c < k{\cdot}Is_a)$ *and* $(Is_a \approx Is_b)$ *and* $(I_0 < I_{min})$	AB
$(Is_a < k{\cdot}Is_b)$ *and* $(Is_b \approx Is_c)$ *and* $(I_0 < I_{min})$	BC
$(Is_b < k{\cdot}Is_a)$ *and* $(Is_c \approx Is_a)$ *and* $(I_0 < I_{min})$	CA
$(Is_c < k{\cdot}Is_a)$ *and* $(Is_a \approx Is_b)$ *and* $(I_0 > I_{min})$	ABG
$(Is_a < k{\cdot}Is_b)$ *and* $(Is_b \approx Is_c)$ *and* $(I_0 > I_{min})$	BCG
$(Is_b < k{\cdot}Is_a)$ *and* $(Is_c \approx Is_a)$ *and* $(I_0 > I_{min})$	CAG
Otherwise	ABC

B. SBS

This method is similar to CBC. However, the disturbance is detected based on the difference between the present sample and that obtained in the previous sampling [8].

C. CUSUM

The CUSUM technique [22] detects disturbances by comparing the sampled current signal values with a drift parameter v, defined as the peak value of the current signal. The algorithm uses two complementary signals ($s1(k)$ and $s2(k)$), obtained from the current samples $s(k)$, defined by [22]:

$$s1(k) = s(k);\ s2(k) = -s(k). \tag{1}$$

Thus, the indexes $g1(k)$ and $g2(k)$ are defined by:

$$g1(k) = max(g1(k-1) + s1(k) - v, 0); \tag{2}$$

$$g2(k) = max(g2(k-1) + s2(k) - v, 0). \tag{3}$$

Finally, a disturbance is detected when one of the indexes ($g1(k)$ or $g2(k)$) exceeds a fixed TH for more than two consecutive samples [22].

D. CSB

This method uses the sum absolute value of the signal slopes considering a 1-cycle window on the analyzed signal [23]. Mathematically, the index $S(k)$ is calculated at instant k by [23]:

$$S(k) = \sum_{l=k-N+1}^{k} d(l), \tag{4}$$

where $d(k)$ is the signal slope at instant k, and N is the number of samples per cycle. A disturbance is detected when the $S(k)$ value exceeds a fixed TH for more than two consecutive samples [23].

IV. EVALUATED FAULT CLASSIFIERS/PHASE-SELECTORS

Concerning the assessed fault classifiers and phase-selectors, six existing approaches were selected, referred to in this paper as 1) Superimposed Current Magnitude-based Classifier (SCM-C) [7], 2) Negative and Zero sequence Current Angle-based Phase-Selector (NZCA-PS) [24], 3) Incremental Torque-based Phase-Selector (IT-PS) [25], 4) Voltage

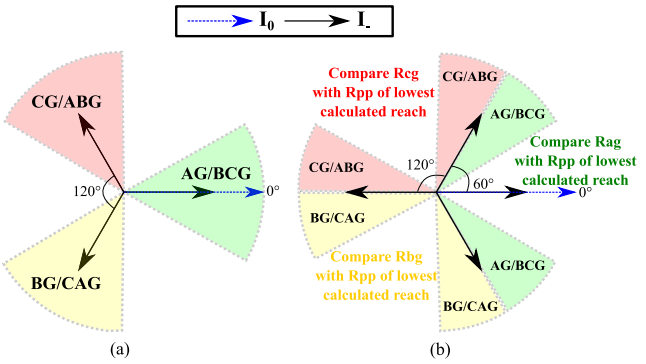

FIGURE 2. Decision-making regions of NZCA-PS.

Magnitude-based Phase-Selector (VM-PS) [6], 5) Negative and Zero sequence Voltage Angle-based Phase-Selector (NZVA-PS) [26], and 6) Voltage Magnitude and Angle-based Classifier (VMA-C) [27].

A. SCM-C

This approach can be used to classify all fault types by comparing the magnitude of the superimposed currents (Is_a, Is_b, and Is_c) and the fundamental zero sequence current (I_0) [7]. The comparisons conducted for the method's decision-making are illustrated in Table 1. Following practices similar to other existing fault classification methods, SCM-C bases its decision on fixed thresholds k and I_{min}, which for the evaluations carried out in this paper are 0.4 and 0.1 p.u. [7], respectively. The $\approx$ symbol means no variation of more than 35% between compared signals.

B. NZCA-PS

NZCA-PS bases its decision-making on the angular difference between the negative and zero sequence currents, according to the regions shown in Fig. 2. If this difference is within the regions of Fig. 2-(a), the distinction between Phase-to-Ground (PG) and Phase-to-Phase-to-Ground (PPG) faults is based on the smallest range calculated by the PG and Phase-to-Phase (PP) loop mho elements [24]. Meanwhile, if the angular difference falls within the regions of Fig. 2-(b), the loop with the lowest estimated resistance distinguishes between PG and PPG faults [24].

This method applies to PG and PPG faults. Some restrictions for the operation based on the levels of negative ($3|\overrightarrow{I_2}| > 0.25|\overrightarrow{I}_n|$) and zero ($3|\overrightarrow{I_0}| > 0.5|\overrightarrow{I}_n|$) sequence currents, compared to the nominal current level ($\overrightarrow{I}_n$), are assumed [24].

C. IT-PS

The IT-PS operates based on the rules depicted in Table 2, assuming three incremental torques [25]:

$$\Delta T_{ab} = Re[\Delta\overrightarrow{V_{ab}} \cdot (1\angle\theta_{L1} \cdot \Delta\overrightarrow{I_{ab}})^*] , \quad (5)$$

$$\Delta T_{bc} = Re[\Delta\overrightarrow{V_{bc}} \cdot (1\angle\theta_{L1} \cdot \Delta\overrightarrow{I_{bc}})^*] , \quad (6)$$

TABLE 2. Decision-making rules of IT-PS.

Conditions	Fault Type
$\Delta T_{ab} > L_{up}$ and $\Delta T_{bc} < L_{low}$ and $\Delta T_{ca} > L_{up}$	AG
$\Delta T_{ab} > L_{up}$ and $\Delta T_{bc} > L_{up}$ and $\Delta T_{ca} < L_{low}$	BG
$\Delta T_{ab} < L_{low}$ and $\Delta T_{bc} > L_{up}$ and $\Delta T_{ca} > L_{up}$	CG
$\Delta T_{ab} > L_{up}$ and $\Delta T_{bc} < L_{int}$ and $\Delta T_{ca} < L_{int}$	AB/ABG
$\Delta T_{ab} < L_{int}$ and $\Delta T_{bc} > L_{up}$ and $\Delta T_{ca} < L_{int}$	BC/BCG
$\Delta T_{ab} < L_{int}$ and $\Delta T_{bc} < L_{int}$ and $\Delta T_{ca} > L_{up}$	CA/CAG
$\Delta T_{ab} > L_{up}$ and $\Delta T_{bc} > L_{up}$ and $\Delta T_{ca} > L_{up}$	ABC

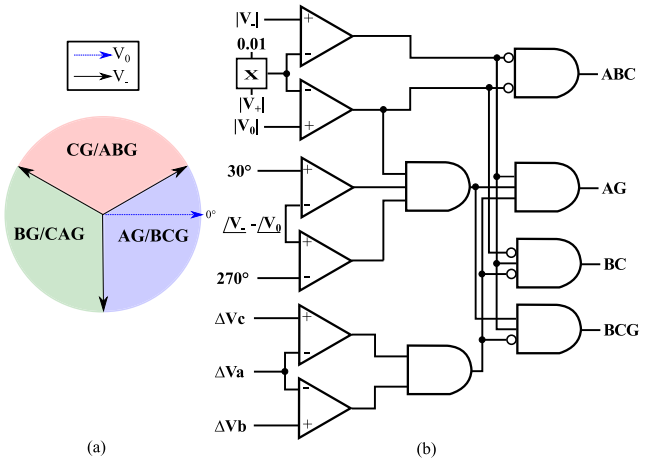

FIGURE 3. VMA-C (a) regions and (b) operational schematic [27].

$$\Delta T_{ca} = Re[\Delta\overrightarrow{V_{ca}} \cdot (1\angle\theta_{L1} \cdot \Delta\overrightarrow{I_{ca}})^*] , \quad (7)$$

where $\Delta\overrightarrow{V_{ab}}$, $\Delta\overrightarrow{V_{bc}}$ and $\Delta\overrightarrow{V_{ca}}$ are incremental voltage phasors, $\Delta\overrightarrow{I_{ab}}$, $\Delta\overrightarrow{I_{bc}}$, and $\Delta\overrightarrow{I_{ca}}$ are incremental current phasors, and θ_{L1} is the line positive sequence impedance angle. The impedance angle of the main overhead lines of the collector circuits was assumed for the analyses ($\approx 74\hat{A}°$).

The distinction between the different fault types is made by comparing the values of ΔT_{ab}, ΔT_{bc}, and ΔT_{ca} normalized by the maximum value among them and the parameters L_{up}, L_{int}, and L_{low}, which represent the method's thresholds. This algorithm applies to PG, PP, PPG, and three-phase (PPP) faults but does not differentiate the ground involvement for two-phase faults. For the performance analyses to be conducted in this paper, $L_{up} = 0.7$, $L_{int} = 0.55$, and $L_{low} = 0.25$ are used [25].

D. VM-PS

This phase-selector is based on two simple steps [6]: 1) A decision threshold is defined based on the loop voltage with the lowest magnitude (AG, BG, CG, AB, BC, or CA, with the magnitude of the phase-to-phase loop voltages divided by $\sqrt{3}$) multiplied by 1.1; 2) The loop voltage (AG, BG, CG, AB, BC, or CA) with a magnitude lower than the defined threshold is selected, indicating the faulted phases. PPP faults are indicated when the AG, BG, and CG loop voltages are simultaneously lower than the threshold. Thus, this method

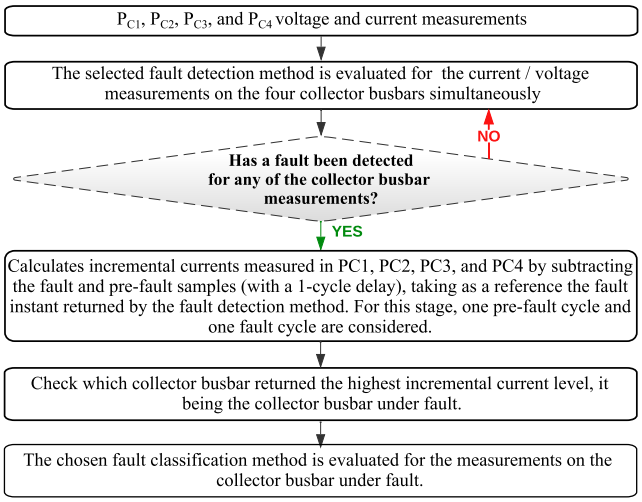

FIGURE 4. Flowchart for measuring management of P_{C1}, P_{C2}, P_{C3}, and P_{C4}.

applies to PG, PP, PPG, and PPP fault types but does not differentiate the ground involvement for two-phase faults [6].

E. NZVA-PS

This method uses the same operating principles as the NZCA-PS but employs voltage signals for its decision-making and applies to PG and PPG faults. It is worth noting that, in [26], operating restriction conditions are not covered for this function as for the current signal-based one. Therefore, such restrictions are not considered for the analyses in this paper.

F. VMA-C

This classifier uses the angular difference between negative and zero sequence voltages, defining three main regions with an angular range of 120°, which indicates AG/BCG, BG/CAG, or CG/ABG faults, as shown in Fig. 3-(a). The fault type is then chosen using the positive, negative, and zero sequence voltage modules, as well as the phase voltage variation magnitudes (ΔV_A, ΔV_B, and ΔV_C), calculated by $\Delta V_\Phi = |V_\Phi| - |V_{\Phi-nominal}|$, where Φ represents the phases A, B, or C. Fig. 3-(b) illustrates the schematic for distinguishing between ABC, AG, AB, and ABG faults, which can also be extended to other fault types [27]. The method applies to all fault types.

V. PERFORMANCE ANALYSIS METHODOLOGY

Firstly, it is worth noting the variety of measuring points available in onshore wind farm collector systems. In particular, measurement points are usually available on the primary of the main collector bus transformers, the secondary of these transformers (collector busbar entrances), and the entrances of the various detailed circuits. Thus, depending on the intended fault diagnosis task, a strategy for selecting the most suitable measurement points is imperative.

In this context, the evaluations of this study are conducted considering two measurement sets. Set 1 covers the

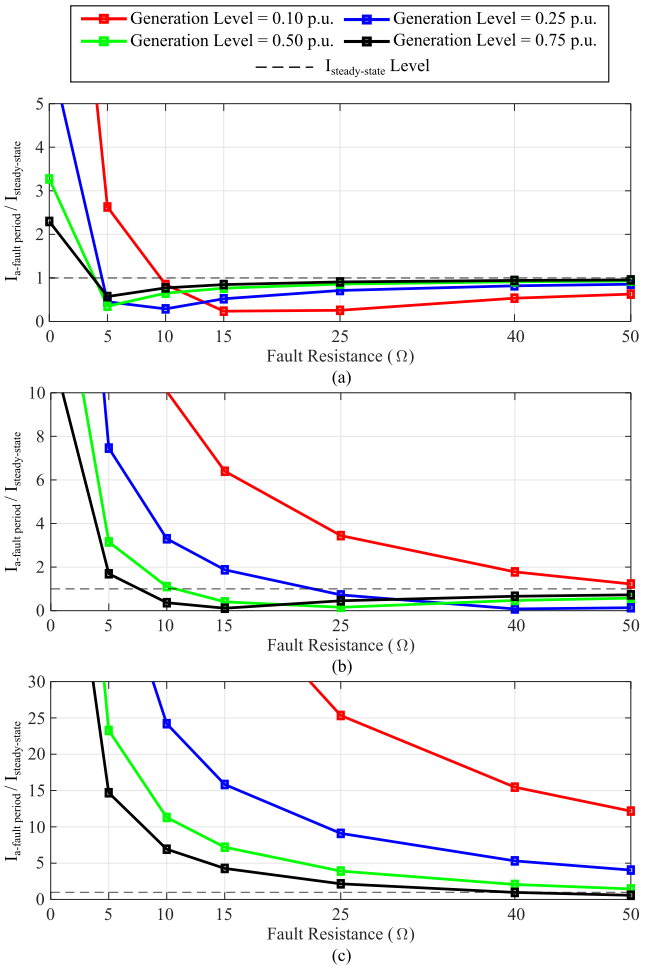

FIGURE 5. Phase A fault current levels measured at (a) P_{MC}, (b) P_{C4}, and (c) at the entrance of the C4 collector busbar detailed circuit, for AG fault at P1-C4 point, with fault resistance variation.

measurements obtained at point P_{MC} as inputs for fault detection and classification methods and aims to detect and classify the fault. Set 2, in turn, employs the measurements at points P_{C1}, P_{C2}, P_{C3}, and P_{C4} as inputs for fault detection and classification methods, following measuring management shown in Fig. 4. In this approach, the collector busbar under fault is identified by presenting the highest levels of incremental current in the faulted phases, thus directing only the measurements from this collector busbar to the fault classification method to be evaluated.

This paper also contributes by explaining why incremental currents are chosen to define the collector busbar under fault. This choice can be justified based on the results shown in Fig. 5, which illustrates how the increase in fault resistance impacts the relationship between the current levels of the faulted phases for fault and steady-state periods for different measurement points. In Fig. 5, this relationship is illustrated for measurements at point P_{MC} (Fig. 5-(a)), P_{C4} (Fig. 5-(b)), and also at the C4 collector busbar's detailed circuit entrance (Fig. 5-(c)), for AG faults applied at point P1-C4 varying the fault resistances.

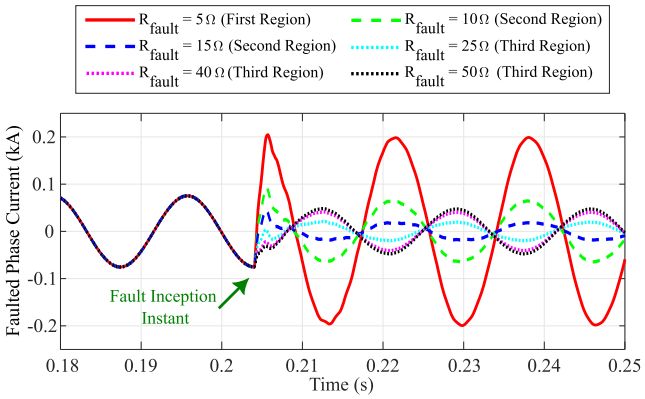

FIGURE 6. Faulted phase current waveforms measured at P_{MC} for AG faults at point P1-C4 with fault resistance variation (Generation Level = 0.1 p.u.).

Considering, for instance, the measurements at P_{MC} (Fig. 5-(a)), three regions of fault current behavior can be highlighted:

- First Region ($I_{a-faultperiod}/I_{steady-state} > 1$ for low fault resistances): This region shows that the fault currents follow conventional patterns, i.e., the phases under fault assume higher levels than the non-faulted phases;
- Second Region ($I_{a-faultperiod}/I_{steady-state} < 1$ for intermediate fault resistances): In this region, the faulted phases' currents are lower than those in the non-faulted phases (steady-state current levels). This situation occurs due to the outfeed condition, i.e., the grid's fault current contribution is reduced enough that it is lower than the load current, resulting in a faulted phase current with lower levels than those obtained in a steady state. However, the P_{MC} point still measures grid contributions to the fault occurring in the wind farm collectors;
- Third Region ($I_{a-faultperiod}/I_{steady-state} < 1$ for high fault resistances): In this region, the faulted phase current increases again, assuming values close to those obtained in the steady state, i.e., the outfeed condition becomes a power loss condition in the phase under fault. In this situation, there is a change in the fault current directionality measured at point P_{MC} so that the grid no longer contributes to the fault in the wind farm collectors.

Fig. 6 complements the results shown in Fig. 5, depicting the waveforms obtained in the faulted phase for AG faults at point P1-C4 with resistance variation, assuming a generation level of 0.1 p.u. The waveforms demonstrate the transition between the previously described three regions.

In this context, the impact of these atypical behaviors on conventional fault diagnosis functions is evident since these functions have their decision-making processes based on identifying the phases under fault as those with the highest or lowest levels for current or voltage-based methods, respectively [6], [7]. In other words, since depending on the fault resistance value, fault currents can assume lower levels than pre-fault ones, besides exhibiting a directionality inversion, significant impacts are expected for conventional fault diagnosis methods.

Therefore, the choice of incremental currents to define the collector busbar under fault is justified since faulted phase currents can be higher or lower than the steady-state currents depending on the behavioral region of the evaluated scenario. This analysis also highlights that the choice of measurement point for fault classification tasks can directly affect the performance of traditional algorithms, which will tend to present satisfactory results only for scenarios with characteristics from the first behavior region ($I_{a-faultperiod}/I_{steady-state} > 1$).

Moreover, once the three behavioral regions have been defined, the influence of the plant's generation level in these regions also stands out since the higher the generation level, the lower the fault resistances required for the transition from the first to the second behavioral region, as well as for the transition from the second to the third region. Finally, by analyzing the results for P_{C4} (Fig. 5-(b)) and also at the entrance to the detailed circuit of collector busbar C4 (Fig. 5-(c)), it can be seen that the closer the measurement point is to the fault point, the greater the fault resistances required for the transition from the first region to the regions of atypical current behavior in the faulted phases (second and third regions).

Finally, it should be emphasized that the TH adjustment of the fault detection methods was strategically defined to favor their performance based on previous analyses of various fault scenarios. Furthermore, the fault classification methods were evaluated 100 ms after the fault was detected, waiting for the estimated phasors to stabilize and the IBR response time [28].

VI. FAULT DETECTION TASK RESULTS AND RECOMMENDATIONS

Fig. 7 shows the success rates for the assessed methods, considering noiseless and noisy signals, voltage and current signals as inputs, and measurements only in P_{MC}. The main findings are:

- The use of current signals as inputs for the methods proved to be more favorable than the use of voltage signals, especially for the CBC (Fig. 7-(a)) and CSB (Fig. 7-(d)) methods, which were positive highlights and the most recommended for this application scenario. Both methods returned 100% accuracy for specific settings for noiseless signals, regardless of the wind farm's generation level. However, it should be noted that these methods had their sensitivity significantly impacted by noise in the signals. For the CBC method, the best setting (TH=0.05) obtained a minimum rate of 100% for noiseless signals and 81.9% for noisy signals. As for the CSB method, the best setting (TH=500) returned a minimum percentage of 100% correct for noiseless signals and 68.5% for noisy signals. Therefore, the authors emphasize the importance of assessing signal noise levels prior to determining the methods' decision thresholds.

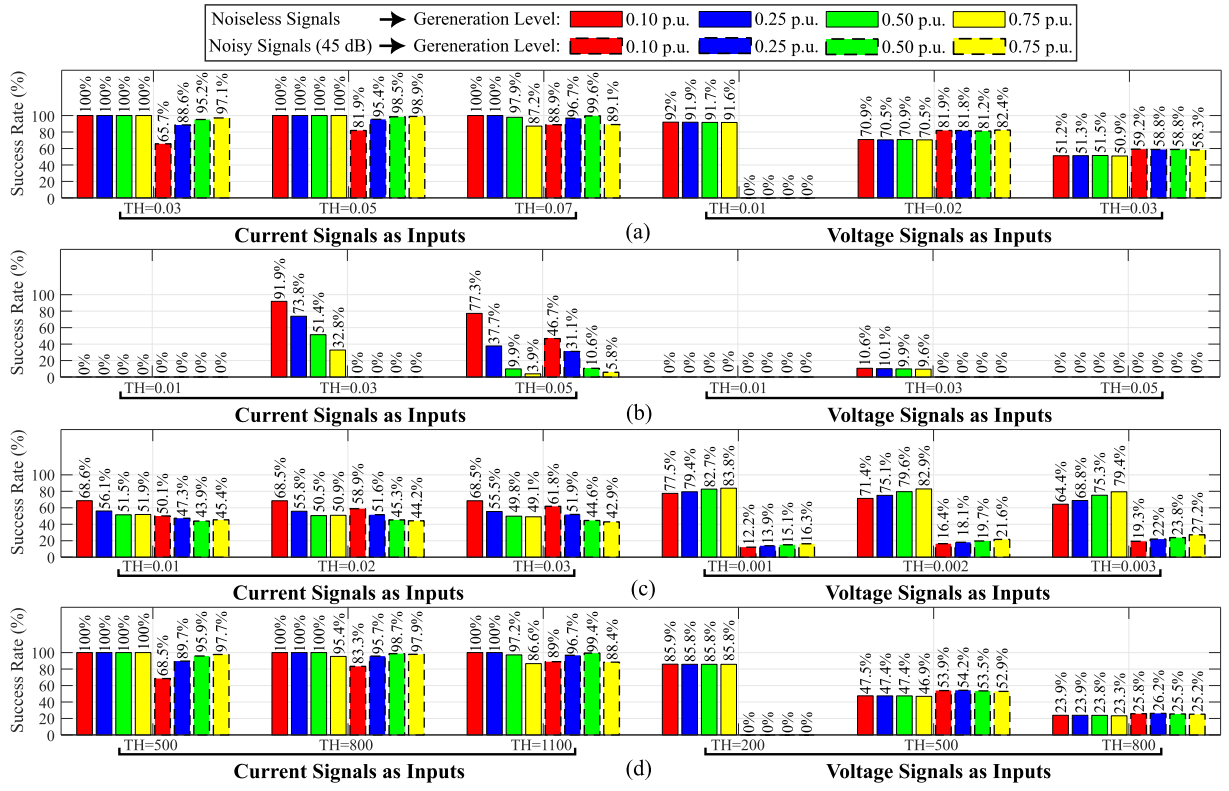

FIGURE 7. Fault detection method's success rates considering (a) CBC, (b) SBS, (c) CUSUM, and (d) CSB, with measurements only on P_{MC}.

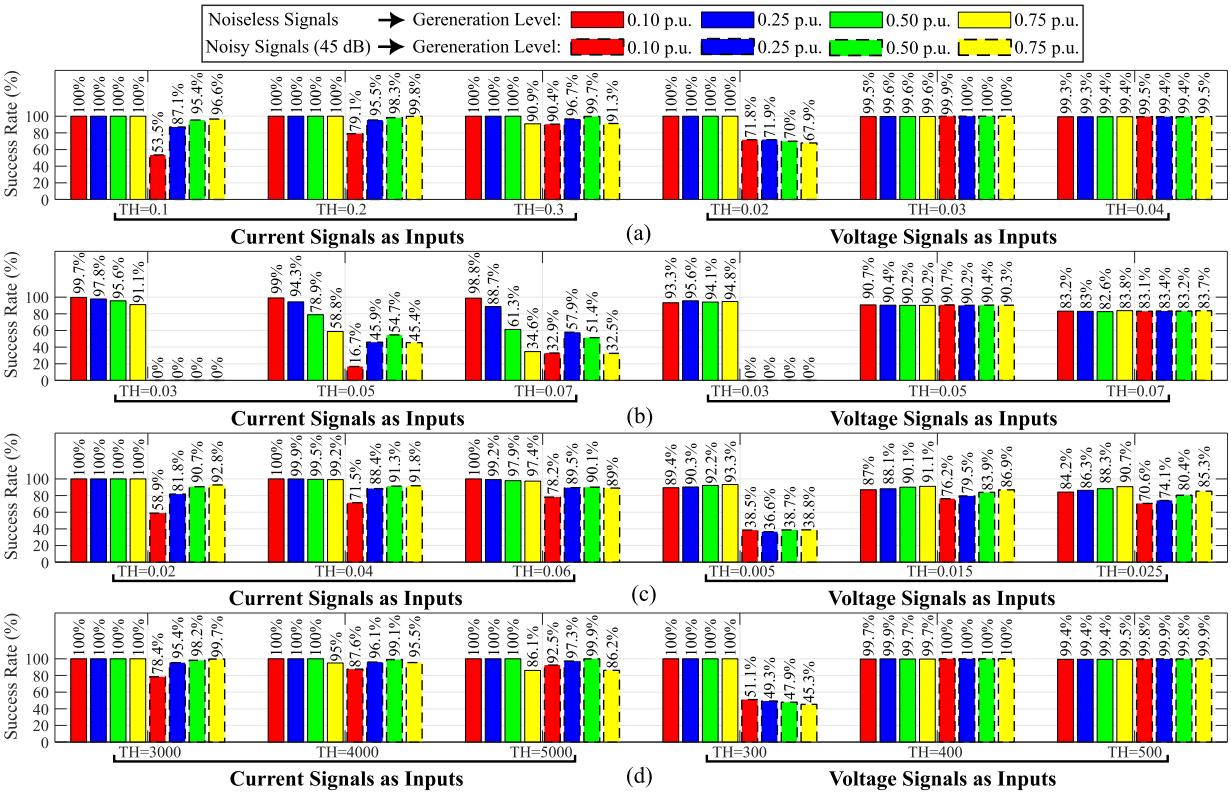

FIGURE 8. Fault detection method's success rates considering (a) CBC, (b) SBS, (c) CUSUM, and (d) CSB, with measurements on the four collector busbars.

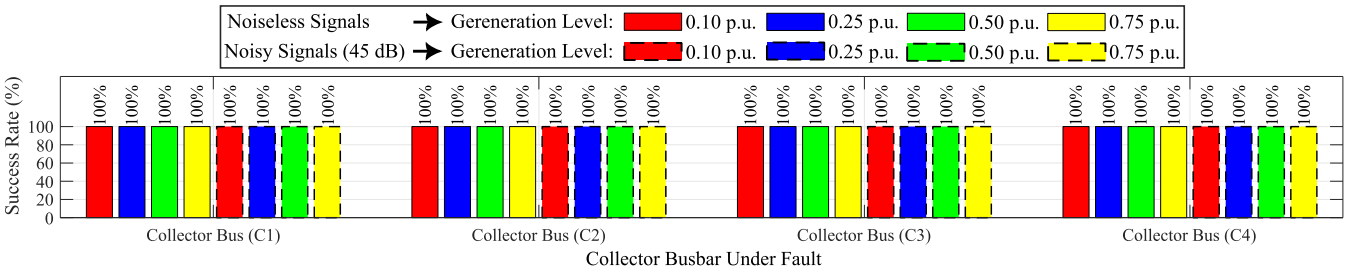

FIGURE 9. Faulty region identification success percentages obtained for each collector busbar, considering the variation in the wind farm's generation level and the presence or absence of signal noise for all the simulated scenarios.

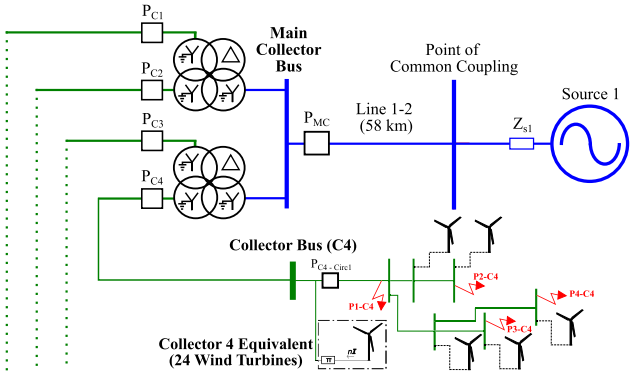

FIGURE 10. Single-line diagram with part of the test system.

- When voltage signals are used as input for the fault detection methods, it can be inferred that the voltage transients are damped by the four-winding transformer, making these signals less suitable for detecting disturbances in the collector busbars for this measurement point. When considering noisy signals, the success rates of the evaluated methods were relatively low. Maximum accuracy percentages of 91.9% and 82.4% were obtained by the CBC method for noiseless and noisy signals, respectively, making it the technique with the most satisfactory performance among the evaluated ones.

When the measurements on the four collector busbars are considered (Fig. 8), along with the management methodology shown in Fig. 4, the conclusions follow:

- Using current signals for fault detection, although there was a general increase in the methods' accuracy, the methods that return the best performances are the same when considering P_{MC} current measurements, and the obtained percentages are quite similar;
- For voltage measurements, maximum accuracy rates close to 100% were obtained, regardless of the presence or absence of noise in the signals, for the CBC and CSB methods. It shows that fault detection using voltage signals is favored when measurements are taken on the collector busbars;
- It is essential to highlight that the TH adjustment significantly influenced the methods' performance, i.e., conventional methods require a careful prior analysis of the test system during disturbances so that the THs can be correctly defined;
- It should also be noted that the measurement management methodology (Fig. 4) combined with voltage signals as inputs for fault detection methods (CBC and CSB methods) were the only combinations that achieved accuracies close to 100% regardless of the power generation level and the presence of noise in the evaluated signals.

In summary, the results recommend using the CSB method (TH = 400), with voltage signals as inputs, for the fault detection task. Finally, the authors point out that applying real-time denoising techniques [29] can be promising to enhance the performance of traditional disturbance detection methods.

VII. REGION IDENTIFICATION RESULTS AND RECOMMENDATIONS

A proposal was presented and justified for identifying the collector busbar under fault based on the incremental currents obtained during the fault period (Fig. 4), assuming access to measurements on the four collector busbars. In this context, this topic seeks to evaluate the performance of this strategy.

The previous analysis showed that the CBC with TH = 0.05 and CSB with TH = 400 methods returned success rates close to 100% for all the evaluated scenarios when considering voltage measurements on the four collector busbars. However, as this topic aims to assess only the strategy in Fig. 4 for identifying the region (collector busbar) under fault, the fault inception instant was assumed to be known. Fig. 9 depicts the success percentages obtained for each collector busbar, considering the variation in the wind farm's generation level and the presence or absence of signal noise for all the simulated scenarios.

The results show that the proposed strategy returned 100% correct identification of the collector busbar under fault and did not have its performance impacted by the presence or absence of noise in the evaluated signals.

In addition to this conclusion, Fig. 5 shows that for measurement points closer to the fault points, higher fault resistances are required to transition the behavior of the currents in the faulted phases from the conventional region

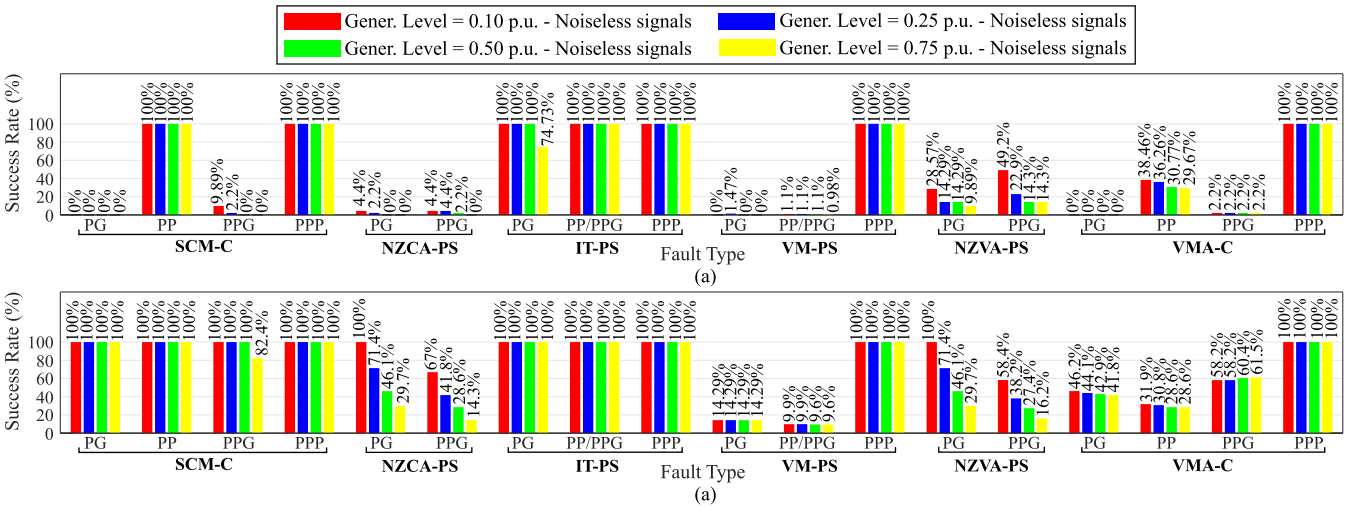

FIGURE 11. Fault classification method's success rates, considering noiseless measurements at (a) P_{MC} and (b) the four collector busbars.

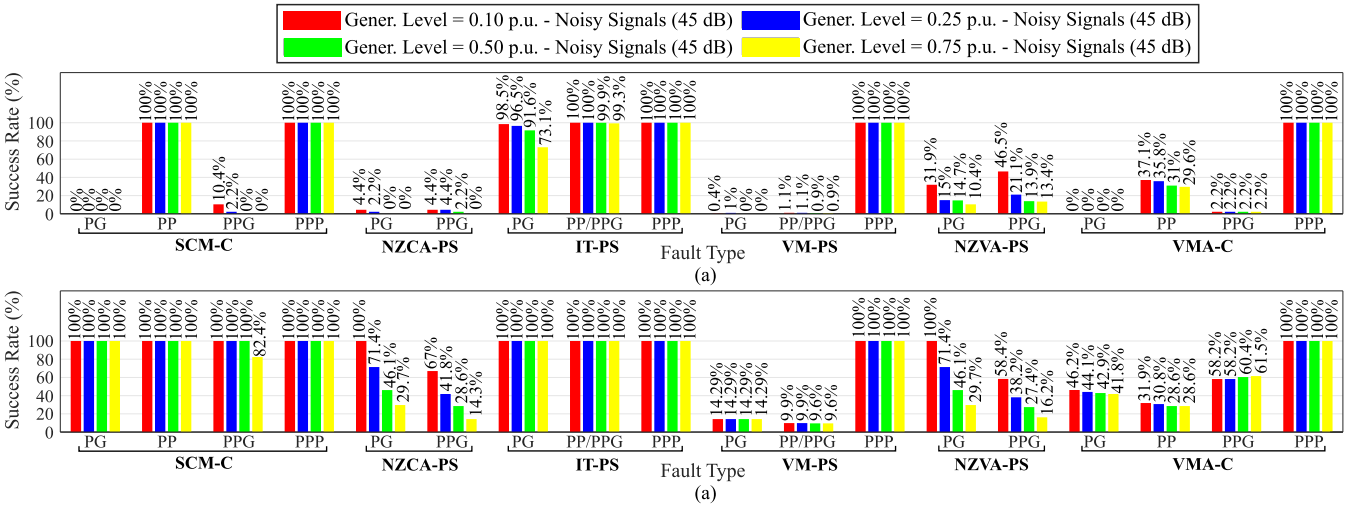

FIGURE 12. Fault classification method's success rates, considering noisy (45 dB) measurements at (a) P_{MC} and (b) the four collector busbars.

(first region) to the non-conventional regions (second and third regions). Therefore, if measurements are available for each of the collector bus circuits (such as the $P_{C4-Circ1}$ measurement point shown in Fig. 10 and its equivalents for the other circuits of this collector bus), the selection strategy shown in Fig. 4 can be extended to select not only the collector busbar under fault but also the circuit of this busbar in which the fault is located. In other words, the strategy that only requires current signals (one pre-fault cycle and one fault cycle) can effectively help with the fault location task in onshore wind farm collector systems.

VIII. FAULT CLASSIFICATION TASK RESULTS AND RECOMMENDATIONS

Fig. 11 shows the success rates for the assessed fault classification methods, considering noiseless signals. The same tests were also carried out considering 45 dB signal noise, and the results are shown in Fig. 12. It is observed that the noise did not significantly affect the accuracy rates returned by the methods. This condition can be justified because the assessed methods are based on fundamental frequency phasors for their operation, and the phasor estimation process filters the signal and dampens a considerable portion of the signal's noisy components.

From the results, the main findings are:

- The methods based exclusively on voltage or current signals' phase angles returned the worst performances and are unsuitable for the fault classification task on wind farm collector systems. This condition can be attributed to the impact of atypical fault currents from the IBRs since for low generation levels (0.1 p.u.), higher success rates were observed for the NZCA-PS and NZVA-PS methods;
- Methods based exclusively on voltage signals (VM-PS and VMA-C) are not suitable for the fault classification in wind farms' collector systems, as they showed

unsatisfactory performance for asymmetrical faults, regardless of the wind farm's generation level or the set of measurements used for the decision-making process;
- There is a general increase in the method's accuracy when measurements on collector busbars are used, emphasizing the influence of the four-winding transformer on the fault classification process (mainly due to its Delta winding, which impacts the system's zero-sequence circuit, besides its impedance, which attenuates variations in the faulted phase signals);
- The results for the SCM-C method especially highlight the influence of zero sequence quantities measured at different points in the system. When measurements were taken at P_{MC}, the method returned 100% accuracy only for faults without ground involvement and reduced percentages for PG and PPG faults. In other words, given that measurements on all collector busbars were used successfully to classify PPG and PP faults and measurements on P_{MC} were only successful for PP faults, identifying ground involvement in faults becomes a challenge when only measurements on P_{MC} are available. However, it can be concluded that when measurements on collector busbars are considered with the measurement management proposal shown in Fig. 4, SCM-C stands out positively, although it still has success rates close to 80% for the maximum generation level and PPG faults;
- The influence of zero sequence quantities on the methods' performance is also confirmed by the high percentages returned by IT-PS for the same conditions since the method ignores the influence of zero-sequence quantities by using quantities between phases in its decision process (ΔI_{ab}, ΔI_{bc}, and ΔI_{ca});
- The IT-PS method was also a positive highlight, especially with the use of measurements on all collector busbars managed by the methodology shown in Fig. 4. However, it should be noted that IT-PS cannot distinguish between PP and PPG faults in the original algorithm. This distinction was also a challenge for the SCM-C method, i.e., it is a complex decision in the context of measuring only P_{MC}.

Aiming to elucidate the challenges of distinguishing ground involvement in faults for measurements only at P_{MC}, Fig. 13 illustrates the ratios between the magnitude of the zero sequence fault current and the nominal current for PG, PP, and PPG faults, considering all the evaluated scenarios. Fig. 13-(b) illustrates a zoom of the boxplots for these relationships, considering noiseless and 45 dB noisy signals, respectively.

When evaluating the results, it can be seen that, in general, the zero sequence currents measured at P_{MC} are similarly negligible for PG, PP, and PPG faults, which makes it challenging to define thresholds for detecting the ground involvement in faults at this measurement point. It should also be noted that noise in the signals makes it impossible to determine a threshold that differentiates PG and PPG faults

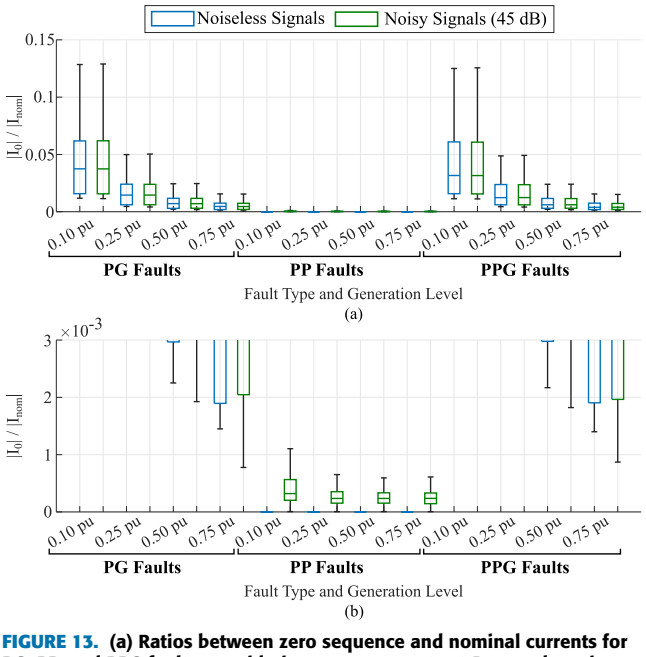

FIGURE 13. (a) Ratios between zero sequence and nominal currents for PG, PP, and PPG faults, considering measurements at P_{MC} and varying wind farm generation levels; (b) zoom area of (a).

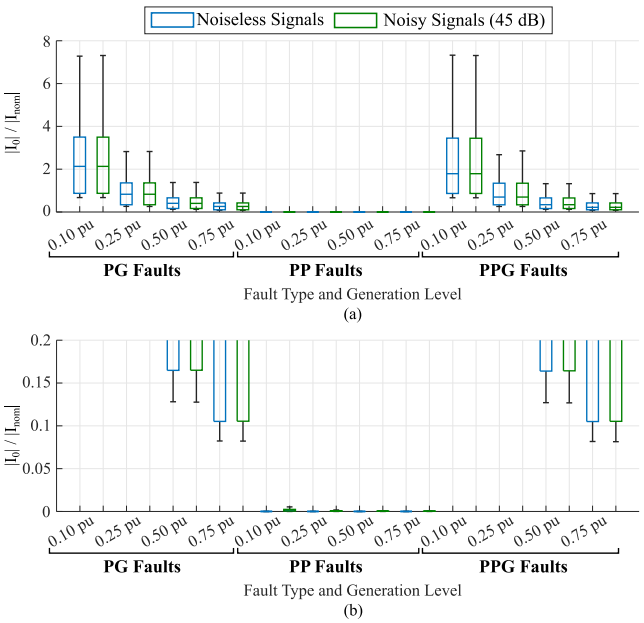

FIGURE 14. (a) Ratios between zero sequence and nominal currents for PG, PP, and PPG faults, considering measurements on collector busbars under fault and varying wind farm generation levels; (b) zoom area of (a).

from PP faults in terms of the measured zero sequence current level.

In contrast, when assessing the same relationships for measurements on faulted collector busbars (Fig. 14), considering the measurement management strategy in Fig. 4, the zero sequence current levels are significantly higher, making it feasible to define a safe threshold for identifying the ground involvement during faults.

In this context, when evaluating the errors obtained for the SCM-C method with a scenario of maximum generation

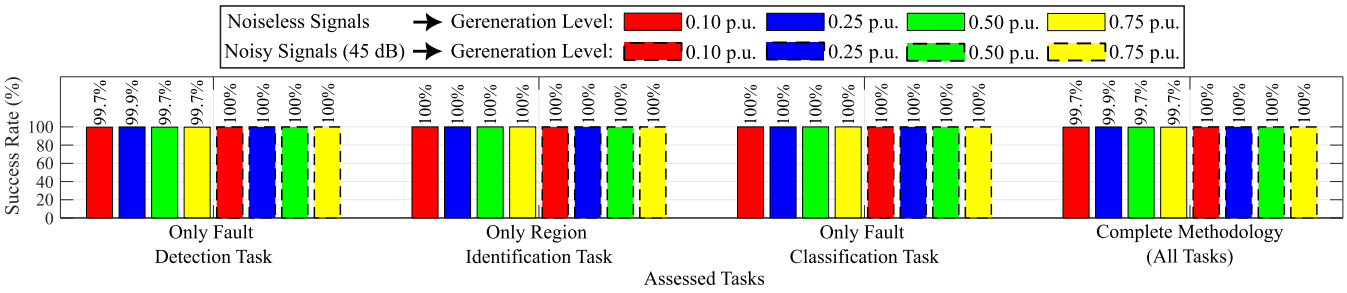

FIGURE 15. Success rates in the fault classification task, by fault type, considering the coordinated operation of the proposed integrated methodology.

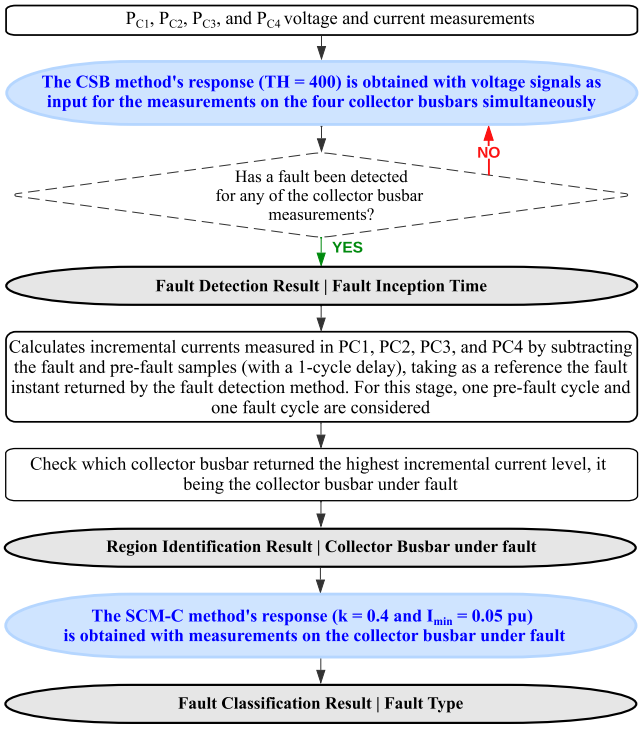

FIGURE 16. Flowchart of the integrated methodology proposed for fault detection, classification and region identification.

at the wind farm and measurements on the four collector busbars, it was observed that these errors are PPG fault scenarios recognized by the algorithm as PP faults. In other words, an analysis of Fig. 14 shows that simply reducing the threshold for recognizing ground involvement in faults from 0.1 to 0.05 is enough for the SCM-C method to return 100% accuracy for all assessed fault types and scenarios.

In conclusion, the results recommend using the SCM-C method, considering the measurements on the collector busbars managed by the strategy proposed in Fig. 4 for classifying faults in onshore wind farm collectors.

IX. PROPOSED FAULT DETECTION, CLASSIFICATION, AND REGION IDENTIFICATION METHODOLOGY

The proposed structure for managing multiple measurements presented in Fig. 4 and the performance assessments conducted in topics VI, VII, and VIII allowed, in addition to the recommendations outlined in the previous topics, the proposal of an integrated methodology for fault detection, classification, and region identification, whose performance validation is depicted in Fig. 15 and the schematic shown in Fig. 16. It is worth emphasizing the pioneering nature of the presented methodology, given that the literature lacks solutions for diagnosing faults within wind power plants, and also due to its practical implementation since it combines conventional fault detection and classification methods with robust and simple strategies for managing measurements and identifying the faulty collector busbar.

For fault detection, the CSB method adjusted with TH = 400 returned minimum success rates of 99.7%, making it the most promising of those evaluated. Identifying the collector busbar under fault also proved very successful, returning 100% accuracy in the conducted analyses. Finally, the SCM-C method was the most promising for the fault classification task, as it is applied to all fault types and also for the high success rates it returned. The study of the zero sequence current levels measured on the collector busbars made it possible to update the I_{min} parameter to a value of 0.05 p.u, enhancing the performance of the SCM-C method for the assessed system.

Fig. 15 illustrates the success rate obtained for the individual tasks (fault detection, classification, and region identification) and the complete methodology operation in a coordinated mode. The results prove the integrated methodology's suitability for fault diagnosis in onshore wind farm collectors.

Moreover, it is important to note that when applying the methodology in Fig. 16 to other onshore wind farms, operators should be aware of the thresholds and parameters of the CSB and SCM-C methods, especially TH for the CSB method and I_{min} for SCM-C, which is still a limitation and an improvement area for the proposed methodology.

X. CONCLUSION

This paper assessed the performance of state-of-the-art fault detection and classification methods using single or multiple measurement points, with multiple measurement points managed by a simple and effective proposal presented in this work. Based on these evaluations, an integrated fault detection, classification, and region identification methodology for onshore wind farm collector systems was also proposed and validated.

Firstly, a pioneering analysis of the fault current behavior in wind farm collector systems was conducted, enabling the definition of three behavior regions not previously found in the related literature. These analyses justified the measurement management approach proposed in the study.

Regarding the fault detection task, the CBC and CSB methods stood out. Both methods returned 100% accuracy for specific settings using noiseless current signals as inputs. However, noisy signals impacted their sensitivity. The best results were achieved using voltage collector busbar measurements managed by the proposal in Fig. 4 and the CSB method (TH = 400), reaching percentages close to 100% for all the assessed scenarios and conditions.

The SCM-C and IT-PS methods returned the most satisfactory performance concerning the fault classification task. However, the IT-PS has limitations due to its impossibility in distinguishing between PP and PPG faults and the limited performance of the SCM-C in classifying PG and PPG faults when adopting measurements at P_{MC}. The best results were achieved using SCM-C and measurements on the collector busbars managed by the proposal in Fig. 4. Moreover, the authors recommended adjusting the ground involvement threshold to obtain 100% accuracy for this method, considering all the evaluated scenarios and conditions.

Thus, the approach to identify the collector busbar under fault proved reliable, returning 100% accuracy. It was inferred that this approach could be extended to identify the collector busbars' circuits on which the fault is located. However, extending the approach requires the availability of current measurements at the entrances of the respective circuits.

Finally, the integrated proposal for fault diagnosis was assessed considering the coordinated operation of the selected fault detection and classification methods and the proposed measurement management strategy. The results prove the effectiveness of the proposed methodology, which is a promising solution for companies responsible for operating wind farms worldwide.

Other areas for improvement or future work include evaluating the methodology for offshore wind farms connected to the grid via High Voltage Direct Current (HVDC) links and proposing an automated methodology for setting the operating thresholds for the fault detection and classification methods comprising the proposed methodology.

REFERENCES

[1] J. Lee and F. Zhao, "Global wind report," Global Wind Energy Council, Brussels, Belgium, Tech. Rep. 2024, 2024.

[2] A. Haddadi, E. Farantatos, I. Kocar, and U. Karaagac, "Impact of inverter based resources on system protection," *Energies*, vol. 14, no. 4, p. 1050, Feb. 2021.

[3] R. Chowdhury and N. Fischer, "Transmission line protection for systems with inverter-based resources—Part I: Problems," *IEEE Trans. Power Del.*, vol. 36, no. 4, pp. 2416–2425, Aug. 2021.

[4] A. Haddadi, M. Zhao, I. Kocar, U. Karaagac, K. W. Chan, and E. Farantatos, "Impact of inverter-based resources on negative sequence quantities-based protection elements," *IEEE Trans. Power Del.*, vol. 36, no. 1, pp. 289–298, Feb. 2021.

[5] M. J. B. B. Davi, M. Oleskovicz, F. V. Lopes, and D. C. Jorge, "Impacts of inverter-interfaced wind power plants in the phase-selection and directional protection functions," *IEEE Latin Amer. Trans.*, vol. 21, no. 1, pp. 151–157, Jan. 2023.

[6] B. Kasztenny, "Line distance protection near unconventional energy sources," in *Proc. 16th Int. Conf. Develop. Power Syst. Protection (DPSP)*, vol. 2022, Mar. 2022, pp. 224–229.

[7] D. V. Coury, M. Oleskovicz, and R. Giovanini, "Digital protection of electrical power systems: From electromechanical relays to intelligent microprocessors," Dept. Elect. Comput. Eng., Univ. São Paulo (EESC-USP), São Carlos, Brazil, 2011, p. 378.

[8] M. Saha, J. Izykowski, and E. Rosolowski, *Fault Location on Power Networks*, vol. 48. New York, NY, USA: Springer, 2010.

[9] N. Ahmed, A. A. Hashmani, S. Khokhar, M. A. Tunio, and M. Faheem, "Fault detection through discrete wavelet transform in overhead power transmission lines," *Energy Sci. Eng.*, vol. 11, no. 11, pp. 4181–4197, Nov. 2023.

[10] C. Saiprakash, S. R. K. Joga, A. Mohapatra, and B. Nayak, "Improved fault detection and classification in PV arrays using stockwell transform and data mining techniques," *Results Eng.*, vol. 23, Sep. 2024, Art. no. 102808.

[11] N. Rosle, N. F. Fadzail, M. I. A. Halim, M. N. K. H. Rohani, M. I. Fahmi, W. Z. Leow, and N. N. A. Bakar, "Fault detection and classification in three phase series compensated transmission line using ANN," *J. Physics: Conf. Ser.*, vol. 1432, no. 1, Jan. 2020, Art. no. 012013.

[12] Y. Zhang, G. He, and G. Li, "Automatic electrical system fault diagnosis using a fuzzy inference system and wavelet transform," *Processes*, vol. 11, no. 8, p. 2231, Jul. 2023.

[13] S. R. Fahim, S. K. Sarker, S. M. Muyeen, M. R. I. Sheikh, and S. K. Das, "Microgrid fault detection and classification: Machine learning based approach, comparison, and reviews," *Energies*, vol. 13, no. 13, p. 3460, Jul. 2020.

[14] A. Swetapadma, A. Yadav, and A. Y. Abdelaziz, "Intelligent schemes for fault classification in mutually coupled series-compensated parallel transmission lines," *Neural Comput. Appl.*, vol. 32, no. 11, pp. 6939–6956, Jun. 2020.

[15] R. Godse and S. Bhat, "Mathematical morphology-based feature-extraction technique for detection and classification of faults on power transmission line," *IEEE Access*, vol. 8, pp. 38459–38471, 2020.

[16] K. A. Kharusi, A. E. Haffar, and M. Mesbah, "Fault detection and classification in transmission lines connected to inverter-based generators using machine learning," *Energies*, vol. 15, no. 15, p. 5475, Jul. 2022.

[17] M. J. B. B. Davi, M. Oleskovicz, and F. V. Lopes, "Exploring the potential of a machine learning-based methodology for fault classification in inverter-based resource interconnection lines," *Electr. Power Syst. Res.*, vol. 223, Oct. 2023, Art. no. 109532.

[18] M. J. B. B. Davi, M. Oleskovicz, and F. V. Lopes, "An impedance-multi-method-based fault location methodology for transmission lines connected to inverter-based resources," *Int. J. Electr. Power Energy Syst.*, vol. 154, Dec. 2023, Art. no. 109466.

[19] E. Muljadi, S. Pasupulati, A. Ellis, and D. Kosterov, "Method of equivalencing for a large wind power plant with multiple turbine representation," in *Proc. IEEE Power Energy Soc. Gen. Meeting*, Aug. 2008, pp. 1–9.

[20] O. Tremblay, R. Gagnon, and M. Fecteau, "Real-time simulation of a fully detailed type-IV wind turbine," in *Proc. Int. Conf. Power Syst. Transients*, 2013, pp. 18–20.

[21] N. W. Miller, J. J. Sanchez-Gasca, W. W. Price, and R. W. Delmerico, "Dynamic modeling of ge 1.5 and 3.6 MW wind turbine-generators for stability simulations," *IEEE Power Eng. Soc. Gen. Meeting*, vol. 3, pp. 1977–1983, Mar. 2003.

[22] S. R. Mohanty, A. K. Pradhan, and A. Routray, "A cumulative sum-based fault detector for power system relaying application," *IEEE Trans. Power Del.*, vol. 23, no. 1, pp. 79–86, Jan. 2008.

[23] K. Nagaraju, P. S. V. S. T. Varma, and B. R. K. Varma, "A current-slope based fault detector for digital relays," in *Proc. Annu. IEEE India Conf.*, Dec. 2011, pp. 1–4.

[24] D. Costello and K. Zimmerman, "Determining the faulted phase," in *Proc. 63rd Annu. Conf. Protective Relay Eng.*, Mar. 2010, pp. 1–20.

[25] G. Benmouyal and J. Mahseredjian, "A combined directional and faulted phase selector element based on incremental quantities," *IEEE Trans. Power Del.*, vol. 16, no. 4, pp. 478–484, 2001.

[26] V. Chakrapani and I. Voloh, "Impact of renewable generation resouce on the distance protection and solutions," in *Proc. 16th Int. Conf. Develop. Power Syst. Protection (DPSP)*, vol. 2022, Mar. 2022, pp. 238–243.

[27] A. Hooshyar, E. F. El.-Saadany, and M. Sanaye-Pasand, "Fault type classification in microgrids including photovoltaic DGs," *IEEE Trans. Smart Grid*, vol. 7, no. 5, pp. 2218–2229, Sep. 2016.
[28] *IEEE Standard for Interconnection and Interoperability of Inverter-Based Resources (IBRS) Interconnecting With Associated Transmission Electric Power Systems*, IEEE Standard IEEE Standard 2800-2022, 2022, pp. 1–180.
[29] W. Wang, J. Li, and S. Lu, "Application of signal denoising technology based on improved spectral subtraction in arc fault detection," *Electronics*, vol. 12, no. 14, p. 3147, Jul. 2023.

MOISÉS J. B. B. DAVI received the degree in electrical engineering and the M.Sc. degree in technological innovation from the Federal University of Triângulo Mineiro, in 2014 and 2021, respectively. He is currently pursuing the Ph.D. degree with the University of São Paulo (EESC-USP), with research in protection and fault diagnosis in systems with inverter-based resources. He has extensive experience in electrical power systems protection, IED commissioning, simulation/analysis of electromagnetic transients, and oscillography analysis. His research interests include protective relaying, power system transients, power system modeling, fault location, and control/protection of renewable energy systems.

MÁRIO OLESKOVICZ (Member, IEEE) received the degree in electrical engineering from the Federal University of Santa Catarina (UFSC), Brazil, in 1995, and the M.Sc. and Ph.D. degrees in electrical engineering from São Carlos Engineering School (EESC), University of São Paulo (USP), Brazil, in 1997 and 2001, respectively. He is currently an Assistant Professor with the Department of Electrical and Computer Engineering (EESC/USP). He works in the electrical engineering area, with a focus on power systems (generation, transmission, distribution, and microgrids), power quality, and power system digital protection.

FELIPE V. LOPES (Senior Member, IEEE) was born in Brazil, in 1985. He is currently a Professor with the Department of Electrical Engineering and Graduate Program on Renewable Energies, Federal University of Paraíba (UFPB), Brazil. He is an Associate Editor of IEEE TRANSACTIONS ON POWER DELIVERY and *Power Engineering Letters* and he is recognized as a Research Productivity Scholar by the Brazilian Council for Scientific and Technological Development (CNPq). Since 2017, he has been involved with activities of the CIGRE B5 study committee in Brazil. In recent years, he has conducted various research on power system transients, electrical grid modeling, fault location, and protection solutions for power networks with conventional and unconventional sources.